Groove-gratings to optimize the electric field enhancement in a plasmonic nanoslit-cavity

Chang Chen (陈昌),[1,2,a)] Niels Verellen,[1,3,4] Kristof Lodewijks,[1,4] Liesbet Lagae,[1,5] Guido Maes,[2] Gustaaf Borghs,[1,5] and Pol Van Dorpe[1,4]

[1]*IMEC vzw., Kapeldreef 75, 3001 Leuven, Belgium*
[2]*Department of Chemistry, Katholieke Universiteit Leuven, Celestijnenlaan 200 F, 3001 Leuven, Belgium*
[3]*Institute for Nanoscale Physics and Chemistry (INPAC), Katholieke Universiteit Leuven, Leuven, B-3001, Belgium*
[4]*ESAT, Katholieke Universiteit Leuven, Kasteelpark Arenberg 10, 3001 Leuven, Belgium*
[5]*Department of Physics and Astronomy, Katholieke Universiteit Leuven, Celestijnenlaan 200 D, 3001 Leuven, Belgium*

We study the spectral properties of a triangular plasmonic nanoslit-cavity with periodic triangular grooves to optimize the field enhancement inside the nanoslit. This work is mainly based on numerical calculations and also partly supported by experimental evidence. In the nanoslit-cavity, we can distinguish following three main contributions to the field enhancement: electrostatic interaction in the nanoslit, surface plasmon polariton standing waves in the cavity and excitation, and reflection of surface plasmon polaritons by the grating. The importance of phase matching between surface plasmons generated at the nanoslit and the gratings is also investigated in order to optimize the local field intensity in the nanoslit. © *2010 American Institute of Physics.*
[doi:10.1063/1.3457017]

I. INTRODUCTION

Nanostructures fabricated by standard micro or nanofabrication processes have become increasingly important in the field of plasmonics[1] because of their widespread applications in molecular spectroscopy [e.g., surface enhanced Raman spectroscopy (SERS) (Refs. 2 and 3) and fluorescence spectroscopy[4]], subwavelength photolithography,[5] and near-field photon manipulations.[6–9] Engineered nanostructures can be exploited to couple, reflect, and focus surface plasmon polaritons (SPPs). Some notable examples are grating structures,[10,11] Fano cavities,[12] dimer antennas,[13] and many more plasmonic nanostructures which give rise to strong field enhancement and a better energy control.

Recently,[14–16] we experimentally demonstrated a plasmonic nanoslit-cavity fabricated on a freestanding membrane: an inverted triangular cavity with a nanoslit at the bottom (primary antenna) and periodic shallow inverted triangular groove gratings surrounding the cavity (secondary antenna). This device was shown to exhibit favorable properties for SERS, as it gives rise to a strong enhancement factor and high spatial resolution. The nanoslit enables to confine SPPs in a localized region and to generate a strongly enhanced field, while the freestanding membrane ensures convenient integration into a biosensor. Similar to nanopore ionic fluidic DNA sequencing, analyte molecules for SERS can be dragged through a nanoslit by electrophoresis.[17,18] When the molecules temporarily appear near the edges of the nanoslit, a corresponding SERS signal can be recorded.

In this paper, we first present a study of the spectral properties of this plasmonic gold nanoslit-cavity. Second, periodic shallow inverted triangular groove gratings surrounding the cavity are introduced. The amount of electromagnetic energy which can be confined in the nanoslit is substantially increased by focusing the SPPs into the nanoslit. Depending on whether a large or small illumination spot is used in a specific application, this can be done by using an optimized grating structure for, respectively, the excitation or reflection of SPPs into the slit. Both numerical calculations based on the finite difference time domain (FDTD) technique and reflection measurements are used to study and optimize the spectral properties of these two types of grating structures. The influence of the pitch, the width and the number of grooves of the gratings as well as SPPs phase matching between the cavity and the grating structures will be discussed in detail.

II. EXPERIMENTAL SECTION

A typical nanoslit-cavity device with gratings is shown in Fig. 1(A). The nanoslit is located at the bottom of a cavity, surrounded with gratings which serve as antennas. This nanodevice was fabricated by standard micromachining processes similar to the work conducted earlier.[19] All of these structures have triangular cross sections with a vertex angle θ of 70.5°, made by KOH wet etching. As shown in Fig. 1(A), the size of the nanoslit depends only on the width of the cavity, as both the thickness of the silicon layer and the metal layers are fixed. The surrounding gratings have following three geometrical parameters: pitch (P), width (W), and distance (L) between the gratings and the cavity. In this work, electron beam lithography, KOH wet etching, and sputter deposition were used to prepare Au gratings with different
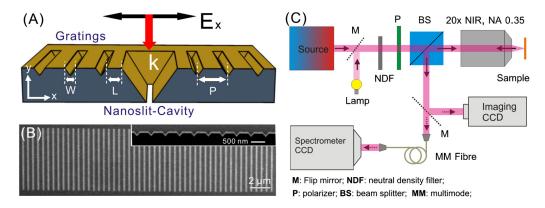
FIG. 1. (Color online) (A) Schematic drawing of the nanoslit-cavity equipped with gratings; the black and red arrows indicate the polarization and propagation directions of the incident light, respectively. (B) SEM images of the grating with 100 grooves with a cross section image in the inset. (C) Schematic drawing of the reflection measurement setup.

widths and pitches for reflection measurements. A scanning electron microscope (SEM) image of gratings with 100 grooves is shown in Fig. 1(B). From the cross section image of the gratings, made by focused ion beam (FIB) cutting, the 100 nm Au layer (bright layer) can clearly be observed. A 5 nm thick Ti adhesion layer between the Si substrate and the Au layer was used.

We have used LUMERICAL FDTD solutions software (from Lumerical Solutions, Inc., Canada) to obtain solutions to Maxwell's equations for the complex geometry of our nanoslit-cavities and groove gratings. These solutions allow us to visualize the electromagnetic modes supported by the devices, to study the electric field enhancement factor $|E_i|^2 = E^2/E_0^2$ (where E_i is the enhancement factor, E is the local electric field, and E_0 is the incident electric field, defined as 1 V/m) inside the nanoslit and to extract the spectral reflection response. To reduce the computational burdens, we assumed a 2D situation [as shown in Fig. 1(A)], which means that the dimensions of the structure are infinite along the out-of-plane axis [z-axis, the longitudinal axis of the device, see Fig. 1(B)]. Several different structures were simulated, including groove gratings, an individual nanoslit-cavity, and a nanoslit-cavity equipped with gratings. The geometrical parameters were chosen to mimic the experimental situation, including the ~5 nm curvature at the edges of the nanoslit. A perfectly matched layer (PML) was used as the radiation boundary condition. PML boundaries in the y direction were placed 1 μm away from the structure while in the x direction the structure layers penetrate through the PML boundaries. The number of PML layers was set to 20 to reduce spurious reflections from the boundaries. The mesh grid size was set to 0.25 nm in the region near the nanoslit and to 3 nm in the region of the gratings and the cavity. The permittivity data for Si were taken from Ref. 20, for Au from Ref. 21, and for Ti from Ref. 22. Although the 5 nm Ti adhesion layer was taken into account in all the simulations, calculations without the adhesion layer indicated that the 100 nm thickness of the Au layer minimizes the influence of Ti on the optical response of the devices which is dominated by surface plasmons on the top Au interface.

The custom-built optical reflection setup is shown in Fig. 1(C). A supercontinuum white light source (Fianium

SC450-4) was used as the source for reflectance spectra. After passing through neutral density filters and a linear polarizer, the beam is focused on the sample surface with a 20× near-infrared (NIR) apochromatic objective (NA=0.35). The reflection from the sample is collected using the same objective and is sent to a spectrometer equipped with a silicon charge coupled device (CCD) array via a multimode fiber (Instaspec X front-illuminated TE cooled CCD 78236 from Newport). All reflection measurements were recorded between 620 and 1100 nm and normalized to the spectrum of a flat Au surface.

III. RESULTS AND DISCUSSION

Due to the fabrication process, the depths of the triangular cavity and grooves only depend on their widths. The geometrical parameters discussed in this work are the width of the nanoslit, the width and the pitch of the gratings, and the distance between the gratings and the cavity. As we discussed before,[14] several aspects contribute to the field enhancement as follows: (1) electrostatic interaction (coupling of SPPs) at the edges of the nanoslit; (2) the Fabry–Pérot-type SPPs resonance inside the cavity (primary antenna); and (3) the SPPs excited or reflected by the gratings (secondary antennas). The size of the nanoslit is crucial but the geometrical parameters of the grating are also important, as they determine the positive or negative contributions of the gratings to the field enhancement.

A. The nanoslit and the triangular cavity

The cavity acts as a resonator for surface plasmons. SPPs are mainly excited by a dipolar excitation of the nanoslit, which is coupled into SPPs on the Au sidewalls. The edges of the top and the bottom convex act as reflectors, enhancing the field enhancement of the nanogap.[23,24] The resonant wavelength depends on the length of the cavity side wall. In this paper, the depth of the Si cavity was fixed at 700 nm (implying a side length of 950 nm), giving rise to a fixed cavity resonance wavelength. We can only change the size of
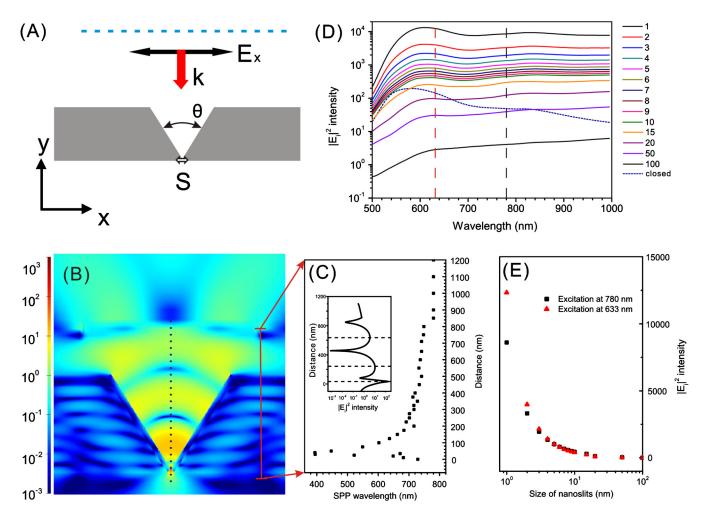
FIG. 2. (Color online) Gap size (s) effect of the nanoslit-cavity without gratings. (A) Schematic drawing of the simulations; reflection spectra are collected behind (blue dashed line) the incident plane wave source. (B) Simulated field enhancement profile in a nanoslit-cavity under 780 nm illumination. (C) The variation in the SPP wavelength inside the cavity; the inset shows a field intensity profile at the symmetry axis of the cavity (black dash line), indicating three standing waves generated inside the cavity. (D) Field enhancement intensity spectra of the nanoslit-cavity (or cavity) for slit sizes ranging from 0 to 100 nm and (E) decay curves of the field enhancement intensity by varying the size of the nanoslit, under 633 nm excitation (red triangular dots) or 780 nm excitation (black square dots).

the nanoslit to vary the efficiency of SPPs coupling inside the nanoslit-cavity and the resulting field enhancement.

The (local) plasmon coupling between the edges of the nanoslit strongly depends on the size of the nanoslit. In simulations, the maximum field enhancement was recorded near the edge of the nanoslit and the reflection spectra were monitored behind the source [as shown in Fig. 2(A)]. The polarization direction of the source was set perpendicular to the longitudinal axis (z axis) of the grooves. A field intensity profile is shown in Fig. 2(B) for a 10 nm nanoslit-cavity illuminated by a plane wave at 780 nm. As mentioned above, a standing wavelike profile is observed. It should be noted that it is a modified Fabry–Pérot cavity: the distance between the side walls decreases gradually along the depth of the slit. For small separations (<200 nm) one can observe a coupling between surface plasmon modes at the metal surfaces of the two side walls, resembling metal-insulator-metal-type waveguide modes.[25] Correspondingly, the mode index increases with respect to single metal/dielectric interfaces. Using the integrated mode solver of LUMERICAL FDTD, we calculated the mode index and subsequently the SPP

wavelength at several positions on the side walls for a free-space wavelength of 780 nm. It is clear on Fig. 2(C), that indeed the SPP wavelength strongly varies in the cavity, certainly near the gap, where the spacing between the side walls is minimal. The inset of Fig. 2(C) shows a field distribution profile at the axis of symmetry of the cavity. The periods in the standing wave pattern clearly shrink along the depth of the cavity. We also monitored the reflection spectra of the nanoslit-cavity with different sizes. All spectra are similar, meaning that the gap size has little or no effect on the SPPs resonance of the cavity.

Due to the "gap effect" in the nanoslit,[26] the field enhancement is almost independent on the wavelength of the excitation as is shown in Fig. 2(D). It is, however, very sensitive to the size of the nanoslit [as shown in Fig. 2(E)]. Similar to the enhancement of dimer particles,[27] the local field enhancement decreases dramatically with increasing gap size. The enhancement of a 1 nm nanoslit is almost five orders higher than that of a 100 nm nanoslit. Unfortunately, it is practically not straightforward to precisely fabricate a 1 nm nanoslit. Our micromachining processes can now rou-

tinely and precisely prepare nanoslits below 10 nm. For field enhancement-based applications such as SERS, larger nanoslits (>10 nm) are less interesting.

B. Gratings for diffractive coupling of surface plasmons

Currently, most examples of focused SPPs for SERS are using periodic hole arrays or slit arrays as the optical antennas.[11] FIB sculpture and electron beam lithography are the most common methods to fabricate these.[10] Here, we prepared gratings with a triangular cross section by silicon anisotropic wet etching, which has following two main advantages: (1) the gratings and the cavity can be simultaneously fabricated by the same etching step and their distance can be well controlled and (2) the nanoslit-cavity device can be mass-produced by standard micromachining processing. The gratings around the cavity were designed to excite, reflect, and focus SPPs into the cavity.

Normally, the maximum physical round-trip distance of SPPs propagating in a grating only depends on the pitch of its grooves. The resonance wavelength (λ_{res}) of the incident light depends on the value of this distance. However, in our triangular grooves, we have to consider the length of the effective optical pathway (EL) between the bottoms of the grooves.[28] As shown in Fig. 3(A), the effective pathway includes the side walls of the grooves and the distance between the top edges of two closed grooves. The EL is given by Eq. (1)

$$EL = P + W \left(\frac{1}{\sin\left(\frac{\theta}{2}\right)} - 1 \right). \tag{1}$$

As the resonance wavelength depends on the effective path length, we can use this equation to predict shifts in the resonance wavelength upon changing the geometry of the grooves.

1. Gratings for excitation of SPPs

In a first strategy, we designed gratings optimized to convert energy from the incident light into SPPs. For wide excitation spots, this allows efficient conversion of the light into SPPs and subsequent focusing into the nanoslit. The efficiency of this process depends strongly on the pitch and the width of the grooves. As shown in Fig. 3(A), in FDTD simulations, reflection spectra were recorded behind the incident plane wave source. A dip in the reflection spectra corresponds to optimal conversion of the light into SPPs.

In the design of groove gratings for the excitation of SPPs, as shown by Eq. (1), the pitch P is the most important parameter since it determines the wavelength of the resonant SPPs. A series of such grooves with W=120 nm and P ranging from 500 to 950 nm was studied both by theoretical calculations and optical reflection experiments. As shown in Fig. 3(B), larger pitches excite SPPs at longer wavelengths. Experimental reflection spectra were obtained from gratings containing 100 grooves and normalized by the spectrum from the flat Au surface. As shown in Fig. 3(C), the resonance dips of gratings with different P are consistent with the

simulated results. The sharp dips appearing at the wavelength corresponding to the grating pitch are caused by Wood's anomalies.[28,29] The apparent absence of the Wood's anomalies phenomenon in the simulations is induced by the integration of the reflected power over the entire simulation width, capturing all diffraction orders. If we monitor the data for fixed angles, we can clearly visualize the Wood's anomaly. We further compared the data from Eq. (1) with results from FDTD and experiments. As shown in Fig. 3(D), the shift trend of resonance wavelengths from these three methods is same, meaning the redshift in the λ_{res} is mainly caused by the extension of EL in the grating with a larger pitch.

For a selected pitch of the gratings, we can also fine tune the SPPs wavelength by changing the width of the grooves. A series of gratings with P=800 nm and W ranging from 100 to 220 nm was studied. As shown in Figs. 3(E) and 3(F), the FDTD simulated resonance wavelengths match well with the experimental ones. Larger groove widths result in an effectively longer optical pathway for SPPs. This, on its turn results in redshifts in λ_{res}. Indeed, the comparison between the effective optical path length and the measured and simulated resonance wavelength shows strikingly similar trend with respect to their dependence on the groove width. Furthermore, we also observe a broadening of the reflection dips for wider grooves. For narrow grooves, with deep-subwavelength dimensions, the pitch is well-defined and a single resonance wavelength can be extracted. Widening the grooves, results in additional retardation between the bottom and the top of the grooves, broadening the resonance and even resulting in additional resonance conditions. This is shown in Fig. 3(E), where for narrow grooves a single dip is observed, while for wide grooves, the dip broadens and additional dips appear. Again, the sharp dips at the grating pitch of 800 nm are caused by Wood's anomalies[29] on the grating structures.

Following the results mentioned above, though Eq. (1) can well explain the shift trend of λ_{res}, we still need full-field electrodynamic calculations to precisely predict λ_{res} of these complex triangular gratings. As shown in Fig. 3(H), this relation between W and P and λ_{res} was obtained by FDTD simulations and compared with the experimental results. It is clear that the simulated results of two grating examples with a width of 120 nm and 170 nm (lines), match well with the corresponding experimental data (dots). This relationship is particularly useful in the design of groove gratings for specific wavelengths. Consider a 780 nm (425 THz) laser, often used in Raman spectroscopy, as an example. As shown in Fig. 3(H), in order to enhance the absorption of the light at 425 THz, several gratings with different W and P are suitable.

2. Gratings for reflection of SPPs

In a second strategy, we focus on gratings that reflect SPPs. This strategy is particularly useful to improve the reflection coefficient of the nanoslit-cavity corners, increasing the optical energy in the nanoslit for small illumination spots. Also in this case the reflection coefficient is mainly determined by the pitch of the grooves. We focused on Bragg
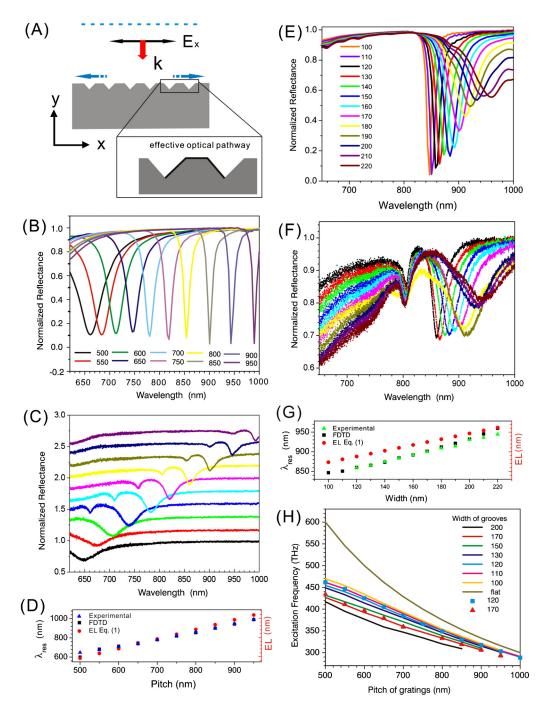
FIG. 3. (Color online) Geometrical effects of gratings on the excitation of SPPs. (A) Schematic drawing of simulations; reflection spectra are collected behind (blue dashed line) the incident plane wave source; the inset shows the definition of the effective optical pathway (black bold line). (B) Simulated and (C) experimental reflection spectra of gratings with W=120 nm and a variable pitch P, normalized to the spectrum of a flat Au surface (offset for clarity) and (D) the corresponding λ_{res} obtained from theoretical calculations and experiments, and EL from Eq. (1). (E) Simulated and (F) experimental reflection spectra of gratings with P=800 nm and a variable width W, normalized to the spectrum of a flat Au surface and (G) the corresponding λ_{res} obtained from theoretical calculations and experiments, and EL from Eq. (1). (H) The relationship between P and W and the excitation light frequency. Lines show simulated data while dots show experimental data.

mirror structures to control the SPPs unidirectional propagation.[11] Experimentally, the reflector role can only be studied by near-field tools such as scanning near field optical microscope (SNOM) or Raman imaging.[11,14] Here, we only discuss simulation results. LUMERICAL FDTD allows the insertion of sources with specific modes, among which also surface plasmon modes. To study the reflection, we inserted a SPP mode propagating in the positive x direction near the gratings [as shown in Fig. 4(A)], with a free-space wave-

length of 780 nm (corresponding to a SPP wavelength, λ_{SPPs}=764 nm on the flat Au surface). The reflected power was collected behind the SPPs source. The reflection was studied for a set of different geometrical parameters of the gratings.

In Fig. 4(B) the dependence of the reflectance on the grating pitch is shown. As expected, a maximum reflectance is observed for P corresponding to half of λ_{SPPs} (P =382 nm, the Bragg condition) and one λ_{SPPs} (P=764 nm).
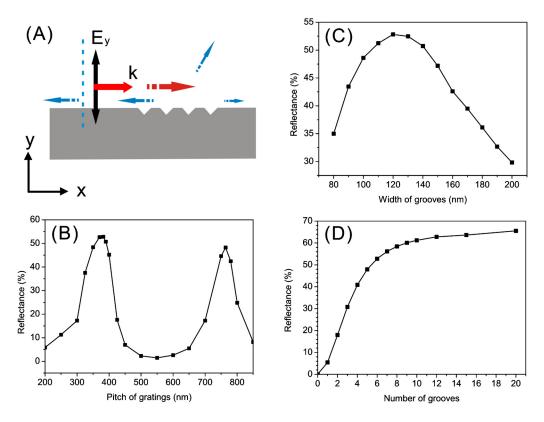
FIG. 4. (Color online) Geometrical effects of gratings on the reflection of SPPs. (A) Schematic drawing of simulations; the red (thick) dashed arrows indicate the input SPPs and the blue (thin) dashed arrows indicate the output SPPs. The excitation wavelength was fixed at 780 nm. The reflected power was collected behind the SPPs source. (B) Reflectance of gratings with six grooves and W=120 nm for varying pitches. (C) Reflectance of gratings with six grooves and P=382 nm for varying widths. (d) Reflectance of gratings with W=120 nm and P=382 nm for increasing numbers of grooves.

Also the width (and thus also the depth) influences the reflection. As shown in Fig. 4(C), a width of 120–130 nm yields a maximum reflection for a pitch of 382 nm. The loss of SPPs propagating into the reflector gratings includes re-emission to the far field and transmission, indicated by the blue (thin) dashed arrows in Fig. 4(A). These losses can be reduced by increasing the amount of grooves in a grating. As shown in Fig. 4(D), increasing the number of grooves for a grating with W=120 nm and P=382 nm yields a better reflection performance. However, as the SPPs decay exponentially during propagation, the amount of grooves actively participating to the effect is limited. Here, we suggest six grooves, the inflexion point of the curve in Fig. 4(D).

3. Phase matching

When combining the groove gratings with the nanoslit-cavity, the distance L between the gratings and the cavity is also important, as it determines how the gratings contribute to the field enhancement inside the nanoslit. Plasmon interference implies that the propagation of SPPs excited or reflected by the gratings should be phase-matched with the standing wave inside the cavity.[11,30]

For devices with a nanoslit-cavity combined with excitation gratings, a plane wave source with a wavelength of 780 nm covering the whole device was used in the simulations. The incoming light is converted into plasmons at following different locations: (1) in the nanoslit-cavity and (2) in the excitation gratings. To generate constructive interference between these two sources, their phases have to be matched. This is clearly indicated in Fig. 5(A), where the field enhancement in the nanogap is shown for different distances L between the nanoslit-cavity and the excitation gratings. Depending on L, a clear enhancement or reduction with respect to the situation without gratings [dashed line in Fig. 5(A)] can be observed. Note that this is the case both for resonant (at 780 nm) or nonresonant excitation. From the diagram in Fig. 3(F) we choose as an example an on-resonance grating with P=680 nm and W=130 nm [black square dots in Fig. 5(A)] and an off-resonance grating with P=500 nm and W=130 nm [red triangular dots in Fig. 5(A)]. The sinusoidal behavior clearly points toward the role of constructive and destructive interference of the two waves. As expected, the maximum enhancement to be obtained from the on-resonance grating is higher than that from the off-resonance grating as can be seen in Fig. 5(A). The periodicity of this effect for the on-resonance gratings is close to λ_{SPPs} (764 nm), while the one of the off-resonance gratings is shorter.

We also simulated the behavior of the combination of nanoslit-cavities with Bragg mirror gratings for incident radiation with wavelengths of 780 nm. We chose this wavelength because it is a commonly used laser line for Raman spectroscopy. In FDTD simulations, a plane wave source with a size of 1 μm was placed above the nanoslit-cavity resulting in a small illumination spot [Fig. 1(A)]. Field enhancement factors are recorded inside the nanoslit. The obtained data are shown in Fig. 5(B). Similar to the gratings for SPPs excitation, depending on the distance between the
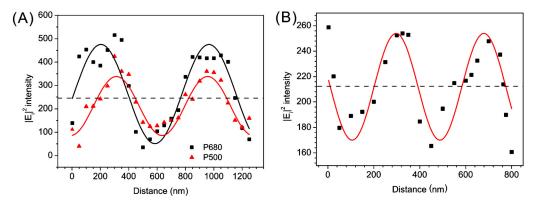
FIG. 5. (Color online) Phase matching effect on the field enhancement intensity, by varying the distance L between the cavity and gratings: (A) gratings for SPPs excitation at 780 nm illumination, an on-resonance grating (P=680 nm, W=130 nm, black square dots) and an off-resonance grating (P=500 nm, W=130 nm, red triangular dots); and (B) Bragg mirror gratings with P=382 nm (for 780 nm excitation) and W=120 nm. The amount of grooves is six and the size of the nanoslit is 10 nm. The dots are simulated data and the lines are sinusoidal fitting. The dashed lines show the field enhancement intensities of the nanoslit-cavity without gratings.

nanoslit-cavity and the grating, the grating can have a positive or negative effect (sinusoidal behavior) on the field enhancement. However, the periodicity is about half of λ_{SPPs} or similar to the pitch of the Bragg mirror gratings.

IV. CONCLUSIONS

This study on the spectral properties of a plasmonic Au nanoslit-cavity equipped with periodic triangular groove gratings explains how propagating SPPs can contribute to the enhancement of the electric field intensity inside the nanoslit-cavity. Two types of gratings were distinguished. A grating for the diffractive excitation of SPPs and a Bragg mirror type grating for the reflection of SPPs back into the nanoslit-cavity to be employed when, respectively, a large (extending far beyond the nanoslit-cavity) or small (focused onto the cavity) illumination spot is used in a specific application. We have shown that besides the commonly discussed crucial parameters such as the pitch and the width (depth) of the gratings, proper phase matching between cavity surface plasmons and grating SPPs has to be considered. This phase matching is easily constructed by tuning the distance between the gratings and the cavity. Depending on this distance, the grating's contribution to the field enhancement can be either positive or negative. Compared to the common square dielectric or metallic gratings widely used in beaming and focusing SPPs,[31] though their spectral properties are similar macroscopically, the triangular gratings or cavities have a better compatibility, a faster manufacturing speed and a larger product capability in the micromachining processing. Considering the wide applications of the manipulation of SPPs, we believe that a good understanding of the spectral properties of this kind of triangular grooves is necessary and important.

ACKNOWLEDGMENTS

[1] A. S. Maier, *Plasmonics: Fundamentals and Applications* (Springer, New York, 2007).
[2] D. R. Ward, N. K. Grady, C. S. Levin, N. J. Halas, Y. P. Wu, P. Nordlander, and D. Natelson, Nano Lett. **7**, 1396 (2007).
[3] M. J. Banholzer, J. E. Millstone, L. D. Qin, and C. A. Mirkin, Chem. Soc. Rev. **37**, 885 (2008).
[4] G. Wrigge, I. Gerhardt, J. Hwang, G. Zumofen, and V. Sandoghdar, Nat. Phys. **4**, 60 (2008).
[5] W. Srituravanich, N. Fang, C. Sun, Q. Luo, and X. Zhang, Nano Lett. **4**, 1085 (2004).
[6] M. Righini, A. S. Zelenina, C. Girard, and R. Quidant, Nat. Phys. **3**, 477 (2007).
[7] A. H. J. Yang, S. D. Moore, B. S. Schmidt, M. Klug, M. Lipson, and D. Erickson, Nature (London) **457**, 71 (2009).
[8] Z. W. Liu, H. Lee, Y. Xiong, C. Sun, and X. Zhang, Science **315**, 1686 (2007).
[9] P. Neutens, P. Van Dorpe, I. De Vlaminck, L. Lagae, and G. Borghs, Nat. Photonics **3**, 283 (2009).
[10] H. J. Lezec, A. Degiron, E. Devaux, R. A. Linke, L. Martin-Moreno, F. J. Garcia-Vidal, and T. W. Ebbesen, Science **297**, 820 (2002).
[11] F. López-Tejeira, S. G. Rodrigo, L. Martín-Moreno, F. J. García-Vidal, E. Devaux, T. W. Ebbesen, J. R. Krenn, I. P. Radko, S. I. Bozhevolnyi, M. U. González, J. C. Weeber, and A. Dereux, Nat. Phys. **3**, 324 (2007).
[12] N. Verellen, Y. Sonnefraud, H. Sobhani, F. Hao, V. V. Moshchalkov, P. Van Dorpe, P. Nordlander, and S. A. Maier, Nano Lett. **9**, 1663 (2009).
[13] D. P. Fromm, A. Sundaramurthy, P. J. Schuck, G. Kino, and W. E. Moerner, Nano Lett. **4**, 957 (2004).
[14] C. Chen, J. A. Hutchison, P. Van Dorpe, R. Kox, I. De Vlaminck, H. Uji-i, J. Hofkens, L. Lagae, G. Maes, and G. Borghs, Small **5**, 2876 (2009).
[15] C. Chen, J. A. Hutchison, F. Clemente, R. Kox, H. Uji-I, J. Hofkens, L. Lagae, G. Maes, G. Borghs, and P. Van Dorpe, Angew. Chem., Int. Ed. **48**, 9932 (2009).
[16] C. Chen, F. Clemente, R. Kox, G. Maes, L. Lagae, G. Borghs, and P. Van Dorpe, Appl. Phys. Lett. **96**, 061108 (2010).
[17] D. Branton, D. W. Deamer, A. Marziali, H. Bayley, S. A. Benner, T. Butler, M. Di Ventra, S. Garaj, A. Hibbs, X. H. Huang, S. B. Jovanovich, P. S. Krstic, S. Lindsay, X. S. S. Ling, C. H. Mastrangelo, A. Meller, J. S. Oliver, Y. V. Pershin, J. M. Ramsey, R. Riehn, G. V. Soni, V. Tabard-Cossa, M. Wanunu, M. Wiggin, and J. A. Schloss, Nat. Biotechnol. **26**, 1146 (2008).
[18] M. Zwolak and M. Di Ventra, Rev. Mod. Phys. **80**, 141 (2008).
[19] R. Kox, C. Chen, G. Maes, L. Lagae, and G. Borghs, Nanotechnology **20**, 115302 (2009).
[20] E. D. Palik, *Handbook of Optical Constant of Solids* (Academic, Orlando, 1985).
[21] P. B. Johnson and R. W. Christy, Phys. Rev. B **6**, 4370 (1972).
[22] D. R. Lide, *CRC Handbook of Chemistry and Physics*, 3rd ed. (CRC, Boca Raton, 2000).
[23] N. M. B. Perney, J. J. Baumberg, M. E. Zoorob, M. D. B. Charlton, S. Mahnkopf, and C. M. Netti, Opt. Express **14**, 847 (2006).
[24] N. M. B. Perney, F. J. G. de Abajo, J. J. Baumberg, A. Tang, M. C. Netti,

M. D. B. Charlton, and M. E. Zoorob, Phys. Rev. B **76**, 035426 (2007).

[25]J. A. Dionne, L. A. Sweatlock, H. A. Atwater, and A. Polman, Phys. Rev. B **73**, 035407 (2006).

[26]E. C. Le Ru, C. Galloway, and P. G. Etchegoin, Phys. Chem. Chem. Phys. **8**, 3083 (2006).

[27]T. Härtling, Y. Alaverdyan, A. Hille, M. T. Wenzel, M. Kall, and L. M. Eng, Opt. Express **16**, 12362 (2008).

[28]T. Søndergaard and S. I. Bozhevolnyi, Phys. Rev. B **80**, 195407 (2009).

[29]Y. W. Jiang, L. D. C. Tzuang, Y. H. Ye, Y. T. Wu, M. W. Tsai, C. Y. Chen, and S. C. Lee, Opt. Express **17**, 2631 (2009).

[30]Z. F. Yu, G. Veronis, S. H. Fan, and M. L. Brongersma, Appl. Phys. Lett. **89**, 151116 (2006).

[31]B. Lee, S. Kim, H. Kim, and Y. Lim, Prog. Quantum Electron. **34**, 47 (2010).